Characterisation of flow behaviour and velocity induced by ultrasound using particle image velocimetry (PIV):

O'Sullivan, Jonathan; Espinoza, Cyrus; Mihailova, Olga; Alberini, Federico

DOI:
10.1016/j.ultsonch.2018.05.037

Document Version
Peer reviewed version

Citation for published version (Harvard):
O'Sullivan, J, Espinoza, C, Mihailova, O & Alberini, F 2018, 'Characterisation of flow behaviour and velocity induced by ultrasound using particle image velocimetry (PIV): Effect of fluid rheology, acoustic intensity and transducer tip size', *Ultrasonics Sonochemistry*, vol. 48, pp. 218-230.
https://doi.org/10.1016/j.ultsonch.2018.05.037

Characterisation of flow behaviour and velocity induced by ultrasound using particle image velocimetry (PIV): Effect of fluid rheology, acoustic intensity and transducer tip size

Jonathan J. O'Sullivan, Cyrus J.U. Espinoza, Olga Mihailova, Federico Alberini

PII: S1350-4177(18)30529-7
DOI: https://doi.org/10.1016/j.ultsonch.2018.05.037
Reference: ULTSON 4195

To appear in: *Ultrasonics Sonochemistry*

Received Date: 3 April 2018
Revised Date: 27 May 2018
Accepted Date: 29 May 2018

Please cite this article as: J.J. O'Sullivan, C.J.U. Espinoza, O. Mihailova, F. Alberini, Characterisation of flow behaviour and velocity induced by ultrasound using particle image velocimetry (PIV): Effect of fluid rheology, acoustic intensity and transducer tip size, *Ultrasonics Sonochemistry* (2018), doi: https://doi.org/10.1016/j.ultsonch.2018.05.037

Characterisation of flow behaviour and velocity induced by ultrasound using particle image velocimetry (PIV): Effect of fluid rheology, acoustic intensity and transducer tip size

Jonathan J. O'Sullivan*, Cyrus J. U. Espinoza, Olga Mihailova, Federico Alberini

School of Chemical Engineering, University of Birmingham, Edgbaston, Birmingham, B15 2TT, UK

** Corresponding author: Email address: j.j.osullivan@bham.ac.uk*

Abstract

Acoustic streaming phenomena of ultrasound propagation through liquid media was investigated experimentally employing particle image velocimetry (PIV). Parameters associated with the ultrasonic processor of ultrasonic amplitude (*i.e.*, acoustic power) and transducer tip diameter (*i.e.*, surface area), as well as, fluid rheology (*i.e.*, water, glycerol solution and CMC solution), were studied for their effects on overall flow behaviour and fluid velocity. PIV yielded velocity gradient maps, demonstrating the acoustic streaming phenomena of ultrasound and its associated flow behaviour as a function of ultrasonic amplitude and fluid rheology, whereby increasing amplitude allowed for greater penetration of the acoustic-beam through the bulk of the fluid, and increasing fluid rheology yielded the converse effect. Moreover, upon impingement of the acoustic-beam with the base of vessel, vortex formation occurred, yielding a recirculation pattern. The maximum observed fluid velocities for water, glycerol solution and CMC solution were 0.329 m s^{-1}, 0.423 m s^{-1}, and 0.304 m s^{-1}, respectively (large diameter sonotrode tip for an ultrasonic amplitude of 80%). Furthermore, shear rates were attained (maximum values of 24.25 s^{-1}), and Reynolds numbers were determined in order to assess the degree of turbulence as a function of investigated parameters.

Keywords: Ultrasound, PIV, Flow behaviour, Velocity characterisation, Newtonian fluids, Non-Newtonian fluids

Highlights

- Acoustic streaming was visualised using particle image velocimetry (PIV).
- Two transducers were investigated with different diameters (3 and 12 mm).
- Three fluids were investigated: water, a glycerol solution and a CMC solution.
- Flow behaviour and velocity magnitudes were assessed for all studied conditions.
- Shear rates and Reynolds number were determined for each of the systems.

1. Introduction

Low frequency (≤100 kHz) high power (>10 W cm^{-2}) ultrasound is a technology which has garnered significant interest over the past decade owing to its capacity to perform a multitude of processing applications [1], including dispersion [2], dissolution [3], molecular modifications [4,5], and emulsification [6,7]. Ultrasonic treatment of liquid media operates through the generation of numerous cavitation sites, arising due to pressure differentials during the propagation of an acoustic wave front through the liquid [8]. The presence of these cavitation bubbles disperse and attenuate ultrasonic waves due to the acoustic impedance differential between the liquid and gaseous phases, causing either partial or complete scattering of these acoustic waves [9]. Cavitation bubbles are located in a small volume at the tip of the sonotrode, whereby the greater the energy input, the greater the number of ultrasonic cavitations [10,11]. Due to the higher number of cavitations concentrated at the base of the sonotrode tip, greater levels of attenuation are observed, which are dominated by acoustic scattering. This results in an exponential decay in acoustic intensity (I_a; W cm^{-2}) with increasing distance from the sonotrode tip, thought to be effectively dissipated at distances as low as 1 cm from the tip [12]. For certain ultrasonic processing batch setups (*e.g.*, 2 L), it is thought that as little as 2% of the volume of liquid is being processed actively situated within the vicinity of the tip [13,14]. Nevertheless, bulk motion does occur for batch processing operations utilising ultrasonics by means of a phenomena known as acoustic streaming [15,16]. The type of acoustic streaming which is observed for power ultrasound applications is referred to as Stuart streaming, first proposed by Lighthill [17], which physically manifests as turbulent acoustic-beams or jets emanating from the tip of a transducer [18].

A detailed understanding of the propagation of these acoustic jets is essential for successful implementation of ultrasound within industrial settings to inform on batch cycle

times and suitable operating conditions (*i.e.*, ultrasonic amplitude). To this end, computational fluid dynamics (CFD) has been employed extensively to investigate the propagation of this phenomena, in order to determine the velocity of the acoustic-beam emanating from the tip and overall bulk mixing in batch processing configurations. Specifically, CFD has been employed to assess both the fluid dynamics and mixing behaviours of ultrasonic processors [11,19–25], and additionally the associated thermal effects of ultrasound in liquid media, due to the chaotic implosion of ultrasonic cavitations [21,26,27]. Xu and co-authors used a numerical approach to simulate velocity distribution of flow from a 490 kHz ultrasonic transducer in water [20]. The effect of transducer power (10 – 50 W), height of transducer with respect to the impedance boundary layer (0.1 – 0.5 m), transducer radius (0.05 and 0.075 m), and absorption coefficient (0.005 and 1 m^{-1}) were factors that were explored. These results highlighted that a maximum velocity of 0.018 m s^{-1} emanated from the base of the transducer, and upon contact with the impedance boundary layer yielded vortex formation adjacent to the acoustic beam, possessing an apparent deadzone [20]. Trujillo and Knoerzer additionally investigated the jet-like flow propagating from ultrasonic transducers using the CFD software package COMSOL [21]. From their results, maximum velocities of 1.95 m s^{-1} were predicted using a Gaussian jet velocity distribution (W/V = 35 kW m^{-3}) [21].

Although significant research has been conducted on the flow behaviour resulting from ultrasound using CFD [11,21], there has been limited research conducted in direct measurement through experimentation of these phenomena. To the authors' knowledge, there are only a few research articles detailing the use of experimentation to assess flow behaviours from ultrasound using either particle image velocimetry (PIV) [25,28,29], laser Doppler anemometry (LDA) [14] or streak photography techniques [30]. PIV is an optical method which relies on tracking the trajectory of tracer particles for the instantaneous measurement

of velocity and other associated properties of fluids in motion (*i.e.*, shear rate or rate of energy dissipation) [31,32]. Schenker and co-authors used an ultrasonic processor with a 25 mm diameter tip (d) operating at an acoustic intensity of 95 ± 5 W cm^{-2} to process 4 L of water [28]. Acoustic streaming was observed emanating from the tip in a conical shape with a maximum velocity magnitude of 0.1 m s^{-1} [28]. These results indicate the presence of deadzones adjacent to the conical sound beam, but are not fully discussed. Additionally, Rahimi and co-authors used PIV as a validation method of CFD results [25]. From their results, the development of conical flow structures were observed emanating from the tip of the transducer of 20 kHz ultrasonic processor, with a diameter of 40 mm. A maximum velocity of 1.98 m s^{-1} was observed up to 0.5 s after activation of the ultrasonic processor immediately under the tip of the sonotrode, and moreover the presence of potential deadzone regions adjacent to the main acoustic jet, similar to the work of Schenker and co-authors and CFD simulations [20,25,28]. LDA is a technique which relies on measuring the Doppler shift of a laser to characterise the velocity of a flowing transparent fluid [33,34]. Kumar and co-authors employed LDA to establish that maximum velocities of 0.225 m s^{-1} were achieved from ultrasonic transducers (P/V = 35 W m^{-3}; d = 13 mm), and that experimental results are in good agreement with CFD predictions [14]. From streak photography experimentation, Cadwell and Fogler reported velocities ranging from 0.7 – 1 m s^{-1} for a low frequency (20 kHz) ultrasonic processor [30]. Moreover, only one fluid, one type of ultrasonic horn and one acoustic intensity were investigated as part of these studies. No systematic investigations of these parameters and their associated interactions are currently available.

The objective of this research was to investigate the propagation of ultrasonic waves through liquid media under different processing conditions, by means of variation of the choice of ultrasonic tip (*i.e.*, diameter) and ultrasonic amplitude (*i.e.*, acoustic intensity), and additionally, fluids exhibiting different physical properties (*i.e.*, Newtonian *vs.* non-

Newtonian liquids, and variation of apparent viscosity), using particle image velocimetry (PIV). From PIV experimentation, velocity gradient maps, local mixing behaviour, fluid velocities, and shear rates were achieved, which possess the capacity to inform manufacturers on operating conditions to achieve optimal processing in terms of acoustic intensity and operation times.

2. Materials and methods

2.1. Materials

Glycerol and sodium carboxymethyl cellulose (CMC; M_w = 700 kDa) were purchased from ReAgent (Cheshire, UK) and Sigma-Aldrich (Dorset, UK), respectively. The seeding particles required for particle image velocimetry (PIV) were 10 µm diameter silver coated hollow glass spheres, and were purchased from Dantec Inc. (UK). The water used in all experiments was passed through a double distillation unit (A4000D, Aquatron, UK).

2.2. Preparation of experimental fluids and rheological characterisation

Three fluids were investigated as part of this study: water, a CMC solution and a glycerol solution. Both CMC and glycerol solutions were prepared using overhead dispersion (RZR 2012, Heidolph, Germany) at 500 rpm with a Rushton disk turbine agitator for a minimum of 4 hours to allow for complete dissolution and dispersion, respectively. The concentration of the CMC and glycerol solutions were 0.25 wt. % and 90 wt. %, respectively.

The viscosity of the glycerol and CMC solutions were measured at 20^{o}C using a HAAKE^{TM} RheoStres^{TM} 1 Rheometer (ThermoFisher Scientific, UK), equipped with a serrated (*i.e.*, minimisation of wall slippage) cup and bob geometry within a shear rate range of 1 – 500 s^{-1}. The glycerol solution demonstrated Newtonian behaviour, whereas the CMC solution exhibited non-Newtonian shear-thinning behaviour according to the power law model as follows:

$$\eta = K\dot{\gamma}^{n-1} \quad (1)$$

Where, $\dot{\gamma}$ is the shear rate (s^{-1}), η is the viscosity (Pa.s), K is the consistency coefficient (-), and n is the power law coefficient (-), whereby the specific K and n values for CMC solution are 0.1215 and 0.784, respectively (R^2 = 0.965) [35].

2.3. Ultrasonic processing conditions and vessel configuration

An ultrasonic processor (Viber Cell 750, Sonics, USA) operating at a frequency of 20 kHz was employed to generate ultrasound for PIV experimentation. Two different stainless steel ultrasonic probes were investigated as part of this study: (1) 12 mm diameter tip and (2) 3 mm diameter microtip. For the larger tip and the microtip, four and three ultrasonic amplitudes were explored, respectively, as detailed in Table 1, whereby the maximum ultrasonic amplitude for both tips was 108 µm, where this information was acquired from the manufacturer of the ultrasonic processor. The acoustic power and acoustic intensity for each tip as a function of ultrasonic amplitude is additionally presented in Table 1, and was determined calorimetrically by measuring the temperature gain as a function of treatment time under adiabatic conditions. The acoustic intensity, I_a (W cm^{-2}), was calculated as follows [36,37]:

$$I_A = \frac{P}{S_A}, where \quad P = m.c_p\left(\frac{dT}{dt}\right) \quad (2)$$

where P_a is the acoustic power (W), S_A is the surface area of the ultrasound emitting surface (cm^2), m is the mass of ultrasound treated fluid (g), c_p is the specific heat of the fluid (kJ/gK) and dT/dt is the rate of temperature change with respect to time, starting at t = 0 (^oC/s). The surface areas for the larger tip and microtip were 1.13 cm^2 and 0.07 cm^2, respectively.

A rectangular borosilicate glass vessel (0.144 m × 0.144 m × 0.144 m) was used for all PIV experimentation, whereby the liquid level was at a height of 0.094 m for water and

CMC solutions, and 0.107 m for the glycerol solution, maintaining a distance of 0.084 m between the tip of the sonotrode and the base of the rectangular vessel. The sonotrode was positioned centrally in the vessel, with an immersion depth of 0.01 m in all instances.

2.4. PIV experimentation and processing of data

PIV experimentation was conducted using a similar approach to that as detailed by Gabriele and co-authors [32] and Espinoza and co-authors [38], with some modifications required for the specific experimental setup in this study, and updates to the PIV setup, as detailed in Fig. 1. The vertical laser plane in all experiments was placed centrally on the ultrasound probe. The two-dimensional (2D) PIV measurements were performed using a TSI PIV system (TSI Inc., USA). The system employed for this study consisted of a dual head 532 nm (green) Nd-YAG laser (Litron Nano PIV, Litron Laser, UK) pulsing at 10 Hz synchronised to a single TSI Power view 4MP (2,048×2,048 pixels) 12 bit CCD (charge-coupled device) camera controlled using a synchroniser (TSI 610035, TSI Inc., USA) attached to a personal computer. The PIV system was controlled using TSI Insight 4G software. Fast Fourier transform (FFT) cross correlation was used to interrogate the two images, which are divided into interrogation areas (IA) of length L_{IA}. The camera was mounted on a computer-controlled traverse.

2D PIV data was acquired for each experimental configuration (*i.e.*, fluid type, transducer tip diameter and acoustic power) and 500 image pairs were taken for each experiment during steady-state acoustic jet conditions [32]. The images were processed employing a Nyquist grid. The dimensions of the IA was 32×32 pixels. Analysis of the PIV output was conducted for the entire volume of the vessel, with the exception of an inconsequential portion at the top of the vessel obscured by the tip of the transducer, which

was mirrored on the other side of the transducer, as shown in Fig. 1 (grey box showing obscured area by sonotrode tip).

The resolution of PIV is dependent upon the scale of the individual IA. Within each IA, the velocity vector obtained is a spatial average. The characteristic length scale, L_{IA}, acts as a filter on the velocity average, since only length scales greater than this scale are resolved. The resolution of smaller length scales requires higher magnification and a CCD camera, requiring the size of the viewing area to be reduced. Thusly, there is a trade-off between the area viewed and the resolution obtained. The resolution adopted was 55.04 – 73.17 µm pixel^{-1} so the measurements were resolved to 1.76 – 2.34 mm for a 32×32 pixel IA. Allowing for a 50% overlap in the IA, the vectors are spaced 0.88 – 1.17 mm apart.

The delay between each frame in an image pair, Δt_d, was chosen in relation to the maximum displacement that a particle could travel in the defined interrogation window. Δt_d can be determined from:

$$\Delta t_d < \frac{M_u Iw}{4U_{tip}} \tag{3}$$

where M_u is the magnification, Iw are the pixel dimensions of the interrogation window and U_{tip} is the velocity emanating from the tip of the ultrasonic transducer (m s^{-1}), which can be calculated using the following expression [21]:

$$U_{tip} = \sqrt{\frac{2K_m}{\rho^2 \pi d^2}}\, e^{[-(r/d)]} \tag{4}$$

where K_m represents the mechanical momentum (kg.m s^{-1}), ρ is the density of the medium (kg m^{-3}), d is the diameter of the transducer tip (m), and r is the radius of the radius of the acoustic jet (m) [17,21]. The delay between two images was adopted assuming that a particle present in the centre of the IA in the first image, moving at maximum observed velocity of $0.5U_{tip}$, is present in the second image with a displacement of $0.25L_{IA}$ [32,39].

During post processing of the vector fields, using the TSI Insight® software, a high pass filter was applied to remove velocities greater than the calculated U_{tip} value, in addition to vectors that were three times greater in magnitude than the standard deviation of the magnitude surrounding vectors in a 9x9 grid.

The application of PIV to systems demonstrating two phases (*i.e.*, liquid and cavitation bubbles) has been previously shown to be problematic by Schenker and co-authors [28], whereby the high density of ultrasonic cavitation bubbles in the vicinity of the sonotrode tip do not allow for observation of separate objects. This is both due to their high density and small size, causing the tracer particles to be invisible within these regions. With increasing distance from the sonotrode tip, the density of ultrasonic cavitations reduces, allowing for practical measurement of the flow behaviour of the fluid [28]. Additionally, it should be noted that the volume affected by the high density of bubbles (*i.e.*, unmeasurable zone) is quite small in comparison to the bulk, possessing a volume as low as 2% in some instances [13,14].

Raw images from PIV experimentation are provided in Fig. 2 for the large diameter tip (*i.e.*, 12 mm) for the 3 investigated fluids (i.e., water, 90 wt. % glycerol solution, and 0.25 wt. % CMC solution) at an ultrasonic amplitude of 80% (*cf.*, Table 1) after steady-state flow has been achieved (*ca.* 3 s after initiation of ultrasound). It can be seen from these images that there is a high density of bubbles in the immediate vicinity of the tip of the transducer making this region invisible to the PIV system, thus, not allowing for the accurate determination of fluid velocities in these regions. It should be noted though that the extent of these regions varies with both investigated fluid (*i.e.*, rheology) and ultrasonic amplitude, hence, no data will be omitted or obscured, rather this phenomenon will be mentioned where relevant throughout the results and discussion.

2.5. Statistical analysis

Student's t-test with a 95% confidence interval was performed using Microsoft Excel and was used to assess the significance of the results obtained, whereby t-test differences with $P < 0.05$ were considered statistically significant.

3. Results and discussions

3.1. Comparison of flow curves of investigated fluids

As part of this study, three fluids were investigated: (1) water, (2) 90 wt. % glycerol solution and (3) 0.25 wt. % CMC solution, and the flow curves of (2) and (3) were initially determined in order to comparatively assess rheological differences between each (Fig. 3), relating these results to each of the ultrasonic processors and investigated amplitudes. Both water [40] and the glycerol solution demonstrated Newtonian rheological behaviour, in contrast to the CMC solution which exhibited non-Newtonian thixotropic rheological behaviour, according to the power law model as previously discussed in Section 2.2. Moreover, significant ($P < 0.05$) rheological differences were observed between the three investigated fluids, whereby the glycerol solution possessed the highest viscosity (0.24 Pa.s at 10 s^{-1}), the CMC solution an intermediate viscosity (0.08 Pa.s at 10 s^{-1}), and water exhibited the lowest value of viscosity (0.001 Pa.s at 10 s^{-1}) [40]. This rheological trend was observed by Mihailova and co-authors, who investigated the flow behaviours of similar fluids (in terms of concentration) through SMX static mixers using positron emission particle tracking (PEPT) [41].

3.2. Effect of ultrasonic amplitude and fluid type on fluid flow behaviour for the ultrasonic transducer with tip diameter of 12 mm

The effect of ultrasonic amplitude (*i.e.*, acoustic intensity; Table 1) within a range of 20 – 80% for the ultrasonic transducer possessing a tip diameter of 12 mm was investigated

for water, whereby the presented results are in the form of velocity gradient maps, normalised with respect to maximum velocity (U_{max}), after the system had achieved steady state flow conditions (*ca.* 3 s; Fig. 3). Table 2 compares the U_{max} of all investigated systems as a function of sonotrode tip diameter, ultrasonic amplitude and studied fluids. In all cases, three key phenomena were observed: (1) the downward trajectory of the acoustic-beam emanating from the tip of the transducer, (2) the formation of vortices upon impact of the acoustic-beam with the base of the vessel allowing for a recirculation behaviour of the fluid, and (3) the presence of stagnant regions above the tip of the ultrasonic transducer (Fig. 4). As ultrasonic amplitude is increased from 20 to 80% there was both a prominent increase in the diameter of the acoustic-beam and greater fluid velocities within the formed vortices, in particular for ultrasonic amplitudes of 60% (Fig. 4c) and 80% (Fig. 4d). The conical geometry of the observed acoustic-beam is consistent with the underlying theory of acoustic streaming for low-frequency, high-power ultrasound systems [17], CFD models of acoustic streaming [11], and PIV visualisation of acoustic streaming [28]. As ultrasonic amplitude was increased from 20 – 80%, there was an increase in the tangential flow with respect to the surface of the tip, allowing for both better vortex formation and recirculation behaviour, and more uniform mixing throughout the vessel (Fig. 4). Additionally, as discussed previously, PIV does not possess the capacity to accurately assess the flow within the volume immediately under the sonotrode tip as the high density of bubbles scatters the PIV laser required for fluid velocity determination (Fig. 4).

The effect of ultrasonic amplitude (20 – 80%) for the ultrasonic transducer with a 12 mm tip diameter on fluid flow behaviour was next investigated for the 90 wt. % glycerol solution, demonstrating Newtonian behaviour with a significantly ($P < 0.05$) greater viscosity than that of water, with results presented in Fig. 5, in the form of velocity gradient maps normalised with respect to maximum velocity (U_{max}; Table 2), after the system had achieved

steady state flow conditions (*ca.* 3 s). At an ultrasonic amplitude of 20%, minimal bulk flow was observed, with flow observed solely within the immediate vicinity of the tip of the ultrasonic transducer (Fig. 5a), attributed to the greater bulk viscosity of the glycerol solution in comparison to water (Fig. 3) generating a greater resistance to fluid flow [41]. As ultrasonic amplitude was increased, greater penetration of the acoustic-beam into the bulk of fluid was achieved, whereby for an ultrasonic amplitude of 40% the degree of penetration had increased by *ca.* 2.5 times (Fig. 5b), for an ultrasonic amplitude of 60% the acoustic-beam started to demonstrate a degree of vortex formation (Fig. 5c), and for an ultrasonic amplitude of 80% the acoustic-beam reached the base of the vessel and displayed more developed vortex formation allowing for enhanced recirculation behaviour (Fig. 5d), comparable to that of water at an ultrasonic amplitude of 20% (Fig. 4a). These significant ($P < 0.05$) differences in observed flow behaviour, as a function of ultrasonic amplitude (20 – 80%), between water and the glycerol solution (90 wt. %), were ascribed to the significant ($P < 0.05$) viscosity differences between the investigated systems (Fig. 3). At low ultrasonic amplitudes (≤ 40%) there is insufficient energy provided to achieve bulk mixing within the vessel, and *ca.* < 10% of the liquid volume is processed, whereas as ultrasonic amplitude is further increased, greater bulk mixing takes place, and the initiation of vortex formation was observed. Furthermore, similar to the previously discussed velocity gradient plots for water (Fig. 4), (1) poor bulk mixing was observed in the volume above the tip of the ultrasonic transducer, (2) a conical profile was observed for the acoustic-beam emanating from the tip of the transducer, and (3) a lack of accurate flow determination in the immediate vicinity of the sonotrode for reasons as previously discussed (Fig. 5).

The effect of a non-Newtonian fluid as a function of increasing amplitude (20 – 80%) was next assessed for the ultrasonic transducer with a tip diameter of 12 mm, whereby the non-Newtonian fluid was a 0.25 wt. % CMC solution, in the form of velocity gradient maps

normalised with respect to maximum velocity (U_{max}; Table 2; Fig. 6), after the system had achieved steady state flow conditions (*ca.* 3 s). Similar results were observed for the CMC solution as that of glycerol, whereby at an ultrasonic amplitude of 20% the acoustic-beam had not achieved full penetration into the bulk fluid (Fig. 6a), comparable to the glycerol solution at an ultrasonic amplitude of 40% (Fig. 5b), and at ultrasonic amplitudes ranging from 40 – 80% the acoustic beam was reaching the base of the vessel and vortex formation was apparent (Fig. 6b-d). This behaviour is in contrast to that of the glycerol solution, and is ascribed to both the significantly ($P < 0.05$) lower viscosity of the CMC solution in comparison to the glycerol solution. The shear-thinning behaviour of the CMC solution promotes greater penetration of the acoustic-beam and enhanced recirculation, as when the ultrasonic amplitude increased, there were increased levels of energy, increasing the shear rate within the system, reducing the bulk viscosity, which is in agreement with the literature for fluid flow within pipes and static mixer systems [42]. Furthermore, the formation of vortices for the CMC solution at an ultrasonic amplitude of 80% (Fig. 6d) was comparable to that of water at an ultrasonic amplitude of 60% (Fig. 4c). In addition, there is a greater volume affected by the high density ultrasonic cavitation region at high ultrasonic amplitudes (60% and 80%), as can be observed from the perceived splitting of the acoustic beam (Fig. 6c and d). Similar to both the velocity gradient plots for water and the glycerol solution, consistent trends were observed in the conical nature of the acoustic-beam, poor bulk mixing in the volume above the tip of the ultrasonic transducer and a lack of accurate fluid flow determination in the volume immediately under the sonotrode tip due to the high density of cavitation bubbles scattering the laser required for PIV measurement (Fig. 6).

These results are in agreement with other studies which have investigated fluid flow utilising either CFD approaches or direct experimental methodologies. For instance, commonalities were observed between the CFD models of Trujillo and Knoerzer, whereby a

conical acoustic-beam was demonstrated emanating from the tip of the sonotrode toward the base of the vessel [21]. However, it should be noted that there is a distinct difference between this CFD prediction and the presented results in this study. Due to the high density of cavitation bubbles in the immediate vicinity under the sonotrode tip this region was invisible to PIV, as previously discussed, thus, the presented results indicated inaccurate low fluid flows (Fig. 4, 5, and 6), whereas the CFD does not exhibit this feature, allowing for a more accurate representation of fluid flow within this region as the presence of a high density of cavitations does not interfere with the model's predictions of flow behaviour. Furthermore, the presented results are consistent with other PIV investigations of the flow behaviour of acoustic streaming phenomena [25,28], such as the conical nature of the acoustic-beam and its downward trajectory, yet the results in these studies do not exhibit the formation of vortices upon impingement of the acoustic-beam with the base of the vessel. Moreover, the results in this study provide a deeper understanding as to the effect of acoustic-jet formation in higher viscosity systems, rather than sole use of water, and utilising a wide range of amplitudes, in addition to a lack of accurate fluid flow determination in the immediate vicinity of the tip of the sonotrode, due to the scattering of laser by high density cavitation regions, as previously discussed [10].

The presented results indicate that an acoustic-beam emanates from the tip of the transducer producing a region of intense mixing within the immediate vicinity under the sonotrode, and the intensity and degree of penetration of the acoustic-beam is highly dependent on the rheological properties of the fluid being processed. Moreover, operation at high ultrasonic amplitudes is advised in all cases, as it provides most efficient processing. In addition, for the experimental setup utilised in this study, a large volume of fluid was studied (> 3L), which is suitable for low viscosity fluids such as water, however, for high viscosity

systems (*i.e.*, 90 wt. % glycerol solution), it is advisable to use a smaller processing volume, aligned with the volume of the acoustic beam, in order to minimise processing times.

3.3. Effect of ultrasonic amplitude and fluid type on fluid flow behaviour for the ultrasonic transducer with tip diameter of 3 mm

The effect of ultrasonic amplitude (20 – 40%; *i.e.*, acoustic intensity; Table 1), and fluid rheology (Fig. 3) was investigated for the ultrasonic processor possessing a tip diameter of 3 mm, whereby the presented results are in the form of velocity gradient maps normalised with respect to maximum velocity (U_{max}; Table 2; Fig. 7). In all cases, similar to the larger diameter sonotrode tip (*i.e.*, 12 mm), the acoustic-beam emanates from the base of the transducer forming a conical profile, whereby the intensity of the beam, and its degree of penetration were dependant on both the ultrasonic amplitude and the fluid rheology.

For water (Fig. 7a-c), the acoustic-beam reached the base of the vessel, and achieved prominent vortex formation in all cases, which is in contrast to the larger diameter tip, whereby comparable trends were observed for an ultrasonic amplitude of 80%, and the results presented by Schenker and co-authors for an ultrasonic probe with a diameter of 25 mm and an acoustic intensity of 95 ± 2.5 W cm^{-2} [28]. The greater mixing behaviour is ascribed to significantly ($P < 0.05$) greater acoustic intensity of the smaller diameter tip in comparison to the larger diameter tip (Table 1), allowing for more efficient mixing behaviour. Moreover, fluid flow was observed in the volume above the tip of the transducer, allowing for more complete mixing of the bulk liquid, which was not achievable for the larger diameter tip (Fig. 4). Although, this could lead to possible segregation within the mixing vessel, yielding variations in material between the bottom and the top of the vessel (Fig. 7). Furthermore, it was observed that with increasing ultrasonic amplitude, a greater intensity of fluid flow was

demonstrated (Fig. 7a-c), which is in agreement with the discussed results for water processed using the larger diameter tip.

For both the glycerol (Fig. 7d-f) and CMC (Fig. 7g-i) solutions, comparable trends were observed as a function of increasing ultrasonic amplitude (20 – 40%), in terms of flow behaviour. At an ultrasonic amplitude of 20% (Fig. 7d and 7g) the acoustic-beam does not reach the base of the vessel, yet weak initiation of the vortex formation occurs, with poor bulk mixing in the volume above the tip of the ultrasonic transducer. As the ultrasonic amplitude was further increased, the acoustic-beam reached the base of the vessel and more prominent vortex formation was exhibited, due to the higher acoustic intensity. The observed flow behaviours were less intense than that of water due to the significantly ($P < 0.05$) higher viscosity values. However, it should be noted, that in contrast to the ultrasonic transducer with the larger diameter tip (12 mm), greater intensity flow was observed in all cases. Interestingly, at ultrasonic amplitudes of 20% and 30%, non-linearity was observed in the acoustic-beam in terms of downward trajectory, whereby the acoustic-beam tended to either direction in the x-plane, regardless of axial orientation of the sonotrode. These variations were thought to be associated with lower ultrasonic amplitudes, and specific initial conditions which dictate the direction of the acoustic-beam, and as the ultrasonic amplitude is further increased these variations did not occur and a prominent downward trajectory of the acoustic-beam was demonstrated. Furthermore, this behaviour is thought to be associated with the elevated viscosity of these systems in comparison to water (Fig. 3), for which it was not observed (Fig. 7a-b), whereby the acoustic-beam would take the path of least initial resistance during activation of the ultrasound, and continue on this trajectory until impingement with the base of the vessel (Fig. 7). Moreover, contact of the acoustic-beam with the base of the vessel, resulting in vortex formation and thus the previously discussed

recirculation behaviour may result in a overall straightening of the acoustic-beam due the axial imbalance.

The obtained results for the ultrasonic transducer with the smaller diameter tip (3 mm; Fig. 7) demonstrated commonalities to the results obtained utilising the larger diameter tip (12 mm), in particular the lack of accurate fluid flow determination within the immediate vicinity of the tip due to the high density of ultrasonic cavities scattering the laser required for PIV measurement, and the recirculation behaviour upon contact with the base of the vessel. The key differences between the investigated systems was the more developed flow behaviour for the smaller diameter tip in comparison to the larger diameter tip, and this behaviour is ascribed to the significantly ($P < 0.05$) higher acoustic intensity of the smaller diameter tip (Table 1).

3.4. Comparative assessment of the performance of the investigated ultrasonic probes

As mentioned previously in section 3.2, the effect of transducer tip diameter (3 and 12 mm), ultrasonic amplitude, and investigated fluid on maximum velocity (U_{max}), is presented in Table 2. There was a general trend, that as ultrasonic amplitude was increased, there was an increase in the values of U_{max}, regardless of investigated fluid or sonotrode (Table 2). This behaviour was attributed to the increasing magnitudes of acoustic intensity (Table 1), providing greater energy to the system allowing for more intense acoustic streaming [17,43]. For the case of the small diameter sonotrode tip (*i.e.*, 3 mm), U_{max} values increased as a function of increasing ultrasonic amplitude for both water and the CMC solution, however in contrast, U_{max} values decreased as a function of increasing ultrasonic amplitude for the case of the glycerol solution (Table 2). This counter-intuitive behaviour is thought to be associated with the volume of the liquid that is affected by the acoustic-beam, whereby for the case of the glycerol solution, as the ultrasonic amplitude was increased, there was an increase in the

volume of fluid processed due to greater penetration of the acoustic-beam within the volume of fluid (Fig. 7). Thus, as a greater volume of fluid was processed with increasing levels of acoustic intensity being distributed throughout these volumes, it manifested as an overall reduction in U_{max}.

The values of U_{max} for the larger diameter transducer tip (*i.e.*, 12 mm) increased for the case of the glycerol solution as a function of increasing ultrasonic amplitude, for the same rationale as previously discussed, however, for both water and the CMC solution, there was an initial increase with increasing ultrasonic amplitude, followed by a decrease after ultrasonic amplitudes of 60% and 40%, respectively. These observed decreases in U_{max} were thought to be associated with the same rationale as for the glycerol solution for the smaller diameter sonotrode tip, greater volume of liquid being processed with increasing ultrasonic amplitudes (Fig. 4 and 6), distributing the acoustic energy throughout a larger volume of fluid, reducing the overall magnitude of U_{max} (Table 2).

When comparing the magnitude of U_{max} between the two investigated transducers, the transducer with the small tip diameter demonstrates significantly ($P < 0.05$) higher magnitudes in U_{max}, in comparison to the transducer with the large tip diameter for the cases of water and the glycerol solution (Table 2), ascribed to the significantly ($P < 0.05$) higher acoustic intensity of the smaller diameter ultrasonic transducer (Table 1). However, for the CMC solution, the opposite trend was observed (Table 2), and this behaviour was thought to be associated with its non-Newtonian character, whereby the its viscosity decreases with increasing acoustic power (*i.e.*, shear rate), in contrast to the other investigated fluids (Fig. 3).

Schenker and co-authors reported a U_{max} value of 0.1 m s^{-1}, determined using PIV [28], and Kumar and co-authors reported a U_{max} value of 0.225 m s^{-1}, achieved employing LDA [14]. The results of Kumar and co-authors are in agreement with those presented in this

study (Table 2), however larger U_{max} values were observed for water, up to 0.339 m s^{-1} for an ultrasonic amplitude of 60% (Table 2). These variations were thought to be associated with differences in the operating conditions employed between the present work and that of Kumar and co-authors [14]. Regarding Schenker and co-authors, significantly ($P < 0.05$) larger values of U_{max} were shown in the present work, similarly thought to be associated with variations in the processing parameters employed (i.e., acoustic intensities and processed volume) [28].

The effect of distance from the transducer tip (1.95 mm, 19.59 mm, 39.13 mm, and 58.69 mm) on fluid velocity directly under the transducer was next explored, in terms of transducer tip diameter, ultrasonic amplitude and investigated fluid, and is shown in Fig. 8, presenting trends in the magnitude of fluid velocity based on the velocity gradient maps as discussed in sections 3.2 and 3.3. Regarding the ultrasonic transducer with the large diameter tip (*i.e.*, 12 mm), within the immediate vicinity of the tip of the transducer the values of velocity are all < 0.1 m s^{-1}, and decrease with increasing ultrasonic amplitude, due to the previously discussed lack of accurate fluid flow determination owing to the high density of ultrasonic cavitations (Fig. 3, 4 and 5), scattering the laser required for effective PIV measurement [38]. As the distance from the tip was increased further, there was an increase in the observed velocity in all cases, with the exception of the glycerol and CMC solutions (Fig. 8c, e) at low amplitudes (*i.e.*, < 40%), as insufficient energy was provided to achieve complete penetration of the bulk fluid, as was observed from the previously discussed velocity gradient maps (Fig. 5 and 6). For water (Fig. 8a), with increasing distance from the transducer tip and increasing amplitude, increasing values of velocity were observed, with the exception of amplitudes of 20% and 40%, whereby the velocity decreased as a function of distance, as insufficient energy was provided to achieved high velocity flow further from the tip of the transducer and these results are in agreement with previously discussed velocity

gradient maps (Fig. 4). The same trend was observed for the glycerol solution (Fig. 8c), whereby the magnitude velocity decreased as a function of distance for ultrasonic amplitudes of 60% and 80%, for the same rationale as described for water. A similar trend was observed for the CMC solution at ultrasonic amplitudes of 20% and 40% (*i.e.*, decreasing fluid velocities as a function of distance from tip of transducer), however, for ultrasonic amplitudes of 60% and 80% there was a continual increase in fluid velocity as a function of distance from the base of the sonotrode (Fig. 8e), and this behaviour was ascribed to both a greater spread of the region of ultrasonic cavitations and increasing fluid velocity due to the shear thinning behaviour of CMC and the increasing levels of power input, as shown in Fig. 6 and previously discussed in section 3.2, respectively.

For the transducer possessing the small diameter tip, for water and the glycerol solution, there is a general trend that as distance from the tip is increased, there is an increase in the fluid velocity, regardless of ultrasonic amplitude (Fig. 8b and d). This behaviour is consistent with the previously discussed velocity gradient maps (Fig. 7). Regarding the CMC solution, there was minimal change in fluid velocity as a function of increasing distance from the transducer tip, rather a marginal decrease in fluid velocity (Fig. 8f), and this was thought to be associated with the non-linear downward trajectory of the acoustic-beam as a function of ultrasonic amplitude (20% and 30%), as previously discussed for the velocity gradient maps (Fig. 7). For the ultrasonic amplitude of 40% for the CMC solution, the fluid velocity remained predominately unchanged as a function of distance from the transducer tip, and this was thought to be associated with the shear-thinning behaviour of the fluid (*Eq.* 1 and Fig. 3), and the narrow acoustic-beam in comparison to the other investigated fluids (Fig. 7).

The theoretical velocity ($U_{theoretical}$) of the acoustic-beam emanating from the transducer tip was determined using *Eq.* 4 [17,43,44], and these values were compared to that of the experimentally determined velocities ($U_{experimental}$) in Table 3. From acoustic streaming

theory, there is thought to be an exponential decay in velocity with both increasing distance from tip and increasing radius of the acoustic-beam cone with increasing distance, and the velocity is independent of fluid rheology [17,43]. Moreover, as the acoustic power is increased, and the fluid density decreased, there was an increase in the magnitude of $U_{theoretical}$ (Table 3). However, there is disagreement between the $U_{experimental}$ and $U_{theoretical}$ results, whereby for the small diameter sonotrode tip the disparity ranges from 2 – 6 times greater for the $U_{experimental}$ values, and the large diameter sonotrode tip the variations are in the order of 1 – 2 magnitudes greater for the $U_{experimental}$ values (Table 3). These differences were thought to be associated with a number of factors, such as (1) a lack of consideration of fluid rheology, which has been shown previously within this study (Fig. 4 - 7) to play a significant role in the development and propagation of the acoustic-beam, and (2) estimations of the acoustic attenuation coefficient, β, a factor which is used for the determination mechanical momentum term (K_m), a value of 3.5 was used in this study based on findings in the literature [45]. These disparities highlight the necessity for the enhancement of the current model (*i.e.*, *Eq.* 4) for determining $U_{theoretical}$ which takes a minimum of fluid rheology into consideration, and potentially other relevant factors.

Shear rate ($\dot{\gamma}$) and Reynolds number (Re) of the acoustic-beam propagating from the tip of the transducer were determined for each of the studied fluids, both investigated transducers and the associated ultrasonic amplitudes, and as a function of distance from the tip of the sonotrode (1.95 mm and 39.13 mm), and are presented in Table 4. Re was determined using the following equation:

$$Re = \frac{\rho U d}{\eta} \tag{5}$$

Where, ρ is the density of the investigated fluid (kg m^{-3}), U is the velocity of the fluid (m s^{-1}), d is the diameter of the acoustic-beam (m), and η is the viscosity of the fluid (Pa.s), whereby

the velocity values were obtained from Table 3, the viscosity of the CMC solution was determined from *Eq*. 1, as a function of shear rate (Table 4), and diameter of the acoustic-beam was determined from the velocity gradient plots (Fig. 3, 4, 5 and 6).

As ultrasonic amplitude was increased, regardless of tip diameter, there is a general trend for the magnitude of the shear rate to increase with all fluids, with the exception of elevated ultrasonic amplitudes within the immediate vicinity of the tip (*i.e.*, 1.95 mm), whereby a high density of ultrasonic cavitations made the accurate determination of velocity, and thus shear rate, problematic as previously discussed. The magnitude of shear rate for the small tip was generally greater than that of the large diameter tip (Table 4), and this behaviour was ascribed to the greater acoustic intensity of the small tip in comparison to that of the large tip (Table 1). Furthermore, the general trend was that the higher viscosity fluids demonstrated higher magnitudes of shear rate thought to be associated with higher rates of viscous dissipation, whereby at an ultrasonic amplitude of 80% for the large tip at a distance from the transducer of 39.13 mm, the shear rate values for the glycerol solution, the CMC solution and water were 18.54 s^{-1}, 17.55 s^{-1}, 14.27 s^{-1}, respectively (Table 4). These trends in shear rate are in agreement with previously discussed velocity data (Table 3 and Fig. 8). In addition, it should be noted that the magnitude of obtained shear rate values (Table 4) is thought to be lower than that of ultrasonic cavitations, as the presented data reflects the shear rate due to both fluid motion (*i.e.*, acoustic streaming), and the lack of accurate fluid flow determination within the immediate vicinity of the tip, rather than collapse of cavitations [1].

Regarding the calculated Reynolds number (*Re*) values, the obtained values were reflective of the velocity of the acoustic-beam (Table 3), diameter of the acoustic-beam (Fig. 4 - 7), and fluid rheology (Fig. 3). Water possessed the highest magnitude *Re* values due to it possessing the lowest viscosity value (Table 4), and as a function of increasing ultrasonic amplitude, regardless of tip diameter, the general trend was for an increase in the magnitude

of *Re*, however, the *Re* values for the large diameter tip were greater than that of the small diameter tip, due to the greater diameter of the acoustic-beam, allowing for a higher degree of turbulence, in particular for the case of water (Table 4). *Re* is indicative of the fluid flow behaviour within a system (*i.e.*, laminar *vs.* turbulent), and the transition between these regimes is highly dependent on the system under investigation (*e.g.*, pipe flow vs. tank agitation) [41,46], thus the determination of flow regime for acoustic streaming is not yet fully possible. Nevertheless, the presented data allows for a greater understanding of the acoustic streaming phenomena and the associated factors which affect the flow regime (Table 4).

4. Conclusions

This study showed that PIV is an effective approach for the assessment of acoustic-beams emanating from sonotrode tips, as a function of fluid rheology (*i.e.*, Newtonian *vs.* non-Newtonian fluids) and ultrasonic processing parameters (*i.e.*, ultrasonic amplitude and sonotrode tip diameter). PIV results were used to assess the flow behaviour, providing insights into the reality of the acoustic streaming phenomena, whereby upon impingement of the acoustic-beam with the base of the vessel, vortex formation occurred yielding a recirculation flow pattern. However, in some instances, dead zones were observed in the volume above the tip of the sonotrode. Moreover, fluid rheology played a significant role in the propagation of the acoustic-beam, where the elevated viscosity of the glycerol solution (90 wt. %) yields poor acoustic-beam penetration at low ultrasonic amplitudes, in contrast to water. From velocity gradient maps, it was possible to both achieve maximum velocity magnitudes, and specific velocities throughout the region of interest, in particular, the speeds immediately under the transducer tip. With increasing distance from the transducer tip, increasing fluid velocities were observed, whereas within the immediate vicinity of the transducer tip, accurate fluid flow was not achievable, ascribed to the high density of

ultrasonic cavitation bubbles in this volume scattering the laser required for PIV measurement. Furthermore, it was demonstrated that higher ultrasonic amplitudes yielded higher shear rates, and higher degrees of turbulence due to the increased fluid velocities. PIV provides insights into the fluid flow resulting from ultrasound, offering useful information to manufacturers for the selection of appropriate processing conditions and efficient design of vessels for ultrasonic processing, and additionally the challenges associated with the processing fluids with either high viscosities or non-Newtonian behaviour.

References

[1] J. O'Sullivan, M. Park, J. Beevers, R. Greenwood, I. Norton, Applications of ultrasound for the functional modification of proteins and nanoemulsion formation: A review, Food Hydrocoll. (2017).

[2] K. Sato, J.-G. Li, H. Kamiya, T. Ishigaki, Ultrasonic Dispersion of TiO2 Nanoparticles in Aqueous Suspension, J. Am. Ceram. Soc. 91 (2008) 2481–2487.

[3] N.A. McCarthy, P.M. Kelly, P.G. Maher, M.A. Fenelon, Dissolution of milk protein concentrate (MPC) powders by ultrasonication, J. Food Eng. 126 (2014) 142–148. doi:10.1016/j.jfoodeng.2013.11.002.

[4] J. O'Sullivan, M. Arellano, R. Pichot, I. Norton, The effect of ultrasound treatment on the structural, physical and emulsifying properties of dairy proteins, Food Hydrocoll. 42 (2014) 386–396.

[5] J. O'Sullivan, B. Murray, C. Flynn, I.T. Norton, The effect of ultrasound treatment on the structural, physical and emulsifying properties of animal and vegetable proteins, Food Hydrocoll. 53 (2016) 141–154.

[6] J. O'Sullivan, B. Murray, C. Flynn, I. Norton, Comparison of batch and continuous

ultrasonic emulsification processes, J. Food Eng. 167(B) (2015) 141–121.

[7] J. O'Sullivan, I. Norton, Novel ultrasonic emulsification technologies, in: P. Williams, G. Phillips (Eds.), Gums Stabilisers Food Ind. 18, The Royal Society of Chemistry, Cambridge, UK, 2016.

[8] G. Servant, J.L. Laborde, A. Hita, J.P. Caltagirone, A. Gérard, Spatio-temporal dynamics of cavitation bubble clouds in a low frequency reactor: comparison between theoretical and experimental results., Ultrason. Sonochem. 8 (2001) 163–74. http://www.ncbi.nlm.nih.gov/pubmed/11441594 (accessed August 21, 2014).

[9] D.J. McClements, Advances in the application of ultrasound in food analysis and processing, Trends Food Sci. Technol. 6 (1995) 293–299. doi:10.1016/S0924-2244(00)89139-6.

[10] S. Martini, Sonocrystallization of Fats, 1st ed., Springer US, New York, 2013.

[11] F.J. Trujillo, K. Knoerzer, Modelling the acoustic field and streaming induced by an ultrasonic horn sonoreactor, in: K. Knoerzer, P. Juliano, P. Roupas, C. Versteeg (Eds.), Innov. Food Process. Technol., 1st ed., Wiley and Sons, Indianapolis, USA, 2011.

[12] M.M. Chivate, A.B. Pandit, Quantification of cavitation intensity in fluid bulk, Ultrason. Sonochem. 2 (1995) S19–S25. doi:10.1016/1350-4177(94)00007-F.

[13] T. Kumaresan, A. Kumar, A.B. Pandit, J.B. Joshi, Modeling Flow Pattern Induced by Ultrasound: The Influence of Modeling Approach and Turbulence Models, Ind. Eng. Chem. Res. 46 (2006) 2936–2950. doi:10.1021/ie060587b.

[14] A. Kumar, T. Kumaresan, A.B. Pandit, J.B. Joshi, Characterization of flow phenomena induced by ultrasonic horn, Chem. Eng. Sci. 61 (2006) 7410–7420. doi:http://dx.doi.org/10.1016/j.ces.2006.08.038.

[15] W.L. Nyborg, Acoustic Streaming due to Attenuated Plane Waves, J. Acoust. Soc. Am. 25 (1953) 68. doi:10.1121/1.1907010.

[16] S. Tjøtta, Theoretical Investigation of Heat and Streaming Generated by High Intensity Ultrasound, Acustica. 85 (1999) 780–787. http://www.ingentaconnect.com/content/dav/aaua/1999/00000085/00000006/art00005 (accessed August 21, 2014).

[17] S.J. Lighthill, Acoustic streaming, J. Sound Vib. 61 (1978) 391–418. doi:10.1016/0022-460X(78)90388-7.

[18] J. Stuart, Unsteady boundary layers, in: L. Rosenhead (Ed.), Laminar Bound. Layers, 1st ed., Oxford University Press, London, 1963.

[19] Z. Wei, L.K. Weavers, Combining COMSOL modeling with acoustic pressure maps to design sono-reactors, Ultrason. Sonochem. 31 (2016) 490–498.

[20] Z. Xu, K. Yasuda, S. Koda, Numerical simulation of liquid velocity distribution in a sonochemical reactor, Ultrason. Sonochem. 20 (2013) 452–459.

[21] F.J. Trujillo, K. Knoerzer, A computational modeling approach of the jet-like acoustic streaming and heat generation induced by low frequency high power ultrasonic horn reactors., Ultrason. Sonochem. 18 (2011) 1263–73. doi:10.1016/j.ultsonch.2011.04.004.

[22] F. Parvizian, M. Rahimi, N. Azimi, A.A. Alsairafi, CFD Modeling of Micromixing and Velocity Distribution in a 1.7-MHz Tubular Sonoreactor, Chem. Eng. Technol. 37 (2014) 113–122.

[23] S.Y. Tang, P. Shridharan, M. Sivakumar, Impact of process parameters in the generation of novel aspirin nanoemulsions – Comparative studies between ultrasound

cavitation and microfluidizer, Ultrason. Sonochem. 20 (2013) 485–497. doi:http://dx.doi.org/10.1016/j.ultsonch.2012.04.005.

[24] B. Sajjadi, S. Asgharzadehahmadi, P. Asaithambi, A.A.A. Raman, R. Parthasarathy, Investigation of mass transfer intensification under power ultrasound irradiation using 3D computational simulation: A comparative analysis, Ultrason. Sonochem. 34 (2017) 504–518.

[25] M. Rahimi, S. Movahedirad, S. Shahhosseini, CFD study of the flow pattern in an ultrasonic horn reactor: Introducing a realistic vibrating boundary condition, Ultrason. Sonochem. 35 (2017) 359–374.

[26] P. Juliano, F.J. Trujillo, G.V. Barbosa-Canovas, K. Knoerzer, The need for thermophysical properties in simulating emerging food processing technologies, in: K. Knoerzer, P. Roupas, C. Versteeg (Eds.), Innov. Food Process. Technol. Adv. Multiphysics Simul., 1st ed., Wiley and Sons, Indianapolis, USA, 2011.

[27] M. Abolhasani, M. Rahimi, M. Dehbani, A.A. Alsairafi, CFD Modeling of Heat Transfer by 1.7 MHz Ultrasound Waves, Numer. Heat Transf. Part A Appl. 62 (2012) 822–841.

[28] M.C. Schenker, M.J.B.M. Pourquié, D.G. Eskin, B.J. Boersma, PIV quantification of the flow induced by an ultrasonic horn and numerical modeling of the flow and related processing times, Ultrason. Sonochem. 20 (2013) 502–509. doi:10.1016/j.ultsonch.2012.04.014.

[29] M. Riccomi, F. Alberini, E. Brunazzi, D. Vigolo, Ghost Particle Velocimetry as an alternative to μPIV for micro/milli-fluidic devices, Chem. Eng. Res. Des. 133 (2018) 183–194. doi:10.1016/J.CHERD.2018.03.005.

[30] M.L. Cadwell, H.S. Fogler, Ultrasonic gas absorption and acoustic streaming observation, in: Chem. Eng. Prog. Symp. Ser. 67, 1971: pp. 124–127.

[31] F. Alberini, L. Liu, E.H. Stitt, M.J.H. Simmons, Comparison between 3-D-PTV and 2-D-PIV for determination of hydrodynamics of complex fluids in a stirred vessel, Chem. Eng. Sci. 171 (2017) 189–203.

[32] A. Gabriele, A.W. Nienow, M.J.H. Simmons, Use of angle resolved PIV to estimate local specific energy dissipation rates for up- and down-pumping pitched blade agitators in a stirred tank, Chem. Eng. Sci. 64 (2009) 126–143.

[33] J.B. Abbiss, T.W. Chubb, E.R. Pike, Laser Doppler anemometry, Opt. Laser Technol. 6 (1974) 249–261.

[34] C. Tropea, Laser Doppler anemometry: recent developments and future challenges, Meas. Sci. Technol. 6 (1995) 605–619.

[35] O. Mihailova, T. Mothersdale, T. Rodgers, Z. Ren, S. Watson, V. Lister, A. Kowalski, Optimisation of mixing performance of helical ribbon mixers for high throughput applications using computational fluid dynamics, Chem. Eng. Res. Des. (2018). doi:10.1016/J.CHERD.2018.01.053.

[36] M.A. Margulis, I.M. Margulis, Calorimetric method for measurement of acoustic power absorbed in a volume of a liquid, Ultrason. Sonochem. 10 (2003) 343–345. doi:http://dx.doi.org/10.1016/S1350-4177(03)00100-7.

[37] J. O'Sullivan, J. Beevers, M. Park, R. Greenwood, I. Norton, Comparative assessment of the effect of ultrasound treatment on protein functionality pre- and post-emulsification, Colloids Surfaces A Physicochem. Eng. Asp. 484 (2015) 89–98. doi:10.1016/j.colsurfa.2015.07.065.

[38] C.J.U. Espinoza, M.J.H. Simmons, F. Alberini, O. Mihailova, D. Rothman, A.J. Kowalski, Flow studies in an in-line Silverson 150/250 high shear mixer using PIV, Chem. Eng. Res. Des. (2018). doi:10.1016/J.CHERD.2018.01.028.

[39] R.J. Adrian, Image shifting technique to resolve directional ambiguity in double-pulsed velocimetry, Appl. Opt. 25 (1986) 3855.

[40] J. Kestin, M. Sokolov, W.A. Wakeham, Viscosity of liquid water in the range −8 °C to 150 °C, J. Phys. Chem. Ref. Data. 7 (1978) 941–948. doi:10.1063/1.555581.

[41] O. Mihailova, D. O'Sullivan, A. Ingram, S. Bakalis, Velocity Field Characterisation of Newtonian and Non-Newtonian Fluids in SMX Mixers Using PEPT, Chem. Eng. Res. Des. (2016). http://www.sciencedirect.com/science/article/pii/S0263876216300119 (accessed March 20, 2016).

[42] O. Mihailova, V. Lim, M.J. McCarthy, K.L. McCarthy, S. Bakalis, Laminar mixing in a SMX static mixer evaluated by positron emission particle tracking (PEPT) and magnetic resonance imaging (MRI), Chem. Eng. Sci. 137 (2015) 1014–1023. http://www.sciencedirect.com/science/article/pii/S000925091500500X (accessed May 9, 2016).

[43] L.K. Zarembo, Acoustic Streaming, in: L.D. Rozenberg (Ed.), High Intensity Ultrason. Fields, 1st ed., Plenum Press, London, 1971.

[44] F.A.A. Fergusson, E.W. Guptill, A.D. MacDonald, Velocity of Sound in Glycerol, J. Acoust. Soc. Am. 26 (1954) 67–69. doi:10.1121/1.1907292.

[45] S. Zhang, H. Jeong, S. Cho, X. Li, Measurement of attenuation coefficients of the fundamental and second harmonic waves in water, in: AIP Conf. Proc., AIP Publishing LLC, 2016: p. 60011. doi:10.1063/1.4940517.

[46] H.S. Yoon, D.F. Hill, S. Balachandar, R.J. Adrian, M.Y. Ha, Reynolds number scaling of flow in a Rushton turbine stirred tank. Part I—Mean flow, circular jet and tip vortex scaling, Chem. Eng. Sci. 60 (2005) 3169–3183. doi:10.1016/J.CES.2004.12.039.

Figure captions

Fig. 1. Schematic overview of PIV and ultrasound experimental setup

Fig. 2. Raw PIV images of (a) water, (b) 90 wt. % glycerol solution, and (c) 0.25 wt. % CMC solution, under steady-state flow conditions (*ca.* 3 s after initiation of ultrasound) for the larger transducer tip (12 mm) at an ultrasonic amplitude of 80%.

Fig, 3. Flow curves for 90 wt. % glycerol solution (solid line) and 0.25 wt. % CMC solution (dashed line), within a shear rate range of 1 – 500 s^{-1}.

Fig. 4. Velocity gradient maps for water, normalised with respect to maximum fluid velocity (U_{max}), as a function of ultrasonic amplitude for the 12 mm ultrasonic transducer: (a) 20%, (b) 40%, (c) 60%, and (d) 80%.

Fig. 5. Velocity gradient maps for 90 wt. % glycerol solution, normalised with respect to maximum fluid velocity (U_{max}), as a function of ultrasonic amplitude for the 12 mm ultrasonic transducer: (a) 20%, (b) 40%, (c) 60%, and (d) 80%.

Fig. 6. Velocity gradient maps for 0.25 wt. % CMC solution, normalised with respect to maximum fluid velocity (U_{max}), as a function of ultrasonic amplitude for the 12 mm ultrasonic transducer tip: (a) 20%, (b) 40%, (c) 60%, and (d) 80%.

Fig. 7. Velocity gradient maps for the 3 mm ultrasonic transducer tip, normalised with respect to maximum fluid velocity (U_{max}) as a function of fluid type and ultrasonic amplitude: (a) water at 20%, (b) water at 30%, (c) water at 40%, (d) 90 wt. % glycerol solution at 20%, (e) 90 wt. % glycerol solution at 30%, (f) 90 wt. % glycerol solution at 40%, (g) 0.25 wt. % CMC solution at 20%, (h) 0.25 wt. % CMC solution at 30%, and (i) 0.25 wt. % CMC solution at 40%.

Fig, 8. Fluid velocity as a function of depth from the tip of the transducer (mm): (a) water for large diameter sonotrode tip, (b) water for small diameter sonotrode tip, (c) glycerol solution for large diameter sonotrode tip, (d) glycerol solution for small diameter sonotrode tip, (e) CMC solution for large diameter sonotrode tip, and (f) CMC solution for small diameter sonotrode tip. ●, ○, ▼, and Δ represent ultrasonic amplitudes of 20%, 40%, 60% and 80%, respectively, for the large diameter sonotrode tip, and ■, □, and ▯ represent ultrasonic amplitudes of 20%, 30% and 40%, respectively, for the small diameter sonotrode tip.

Figures

Fig. 1.

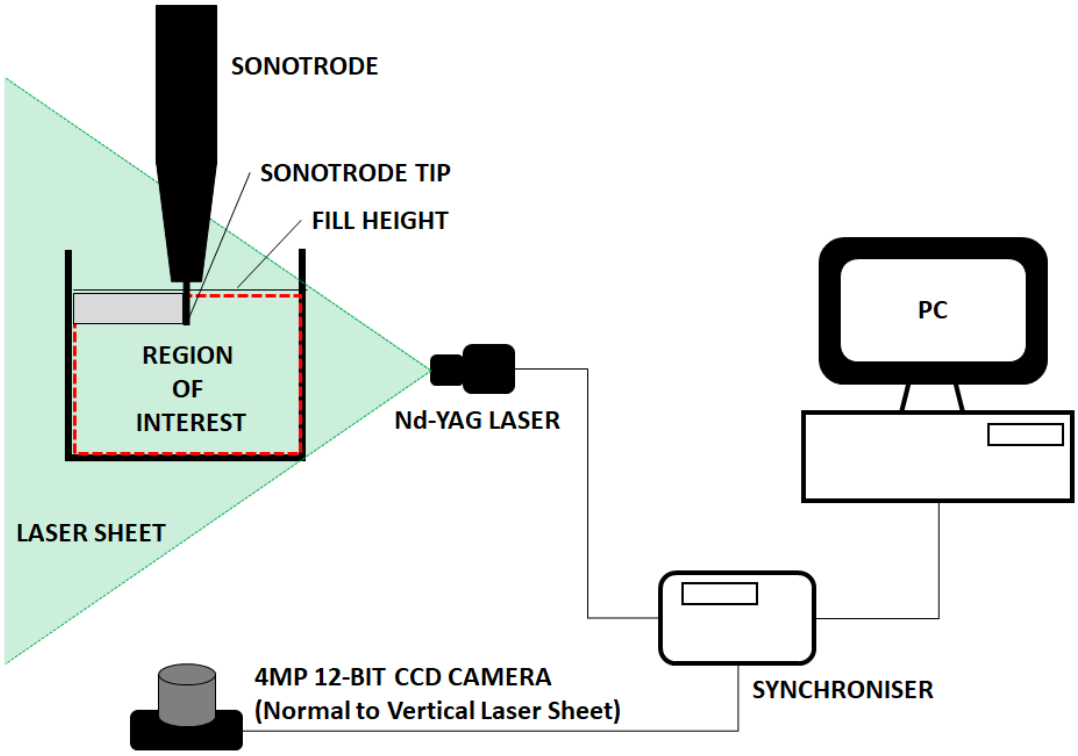

Fig. 2.

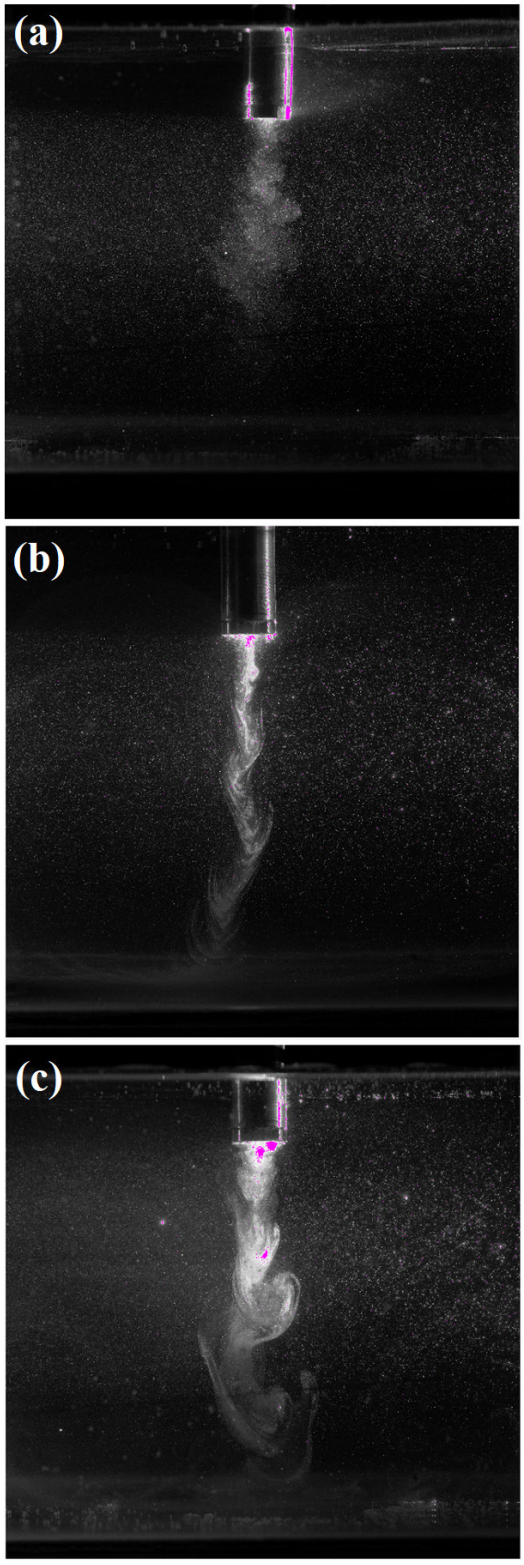

Fig. 3.

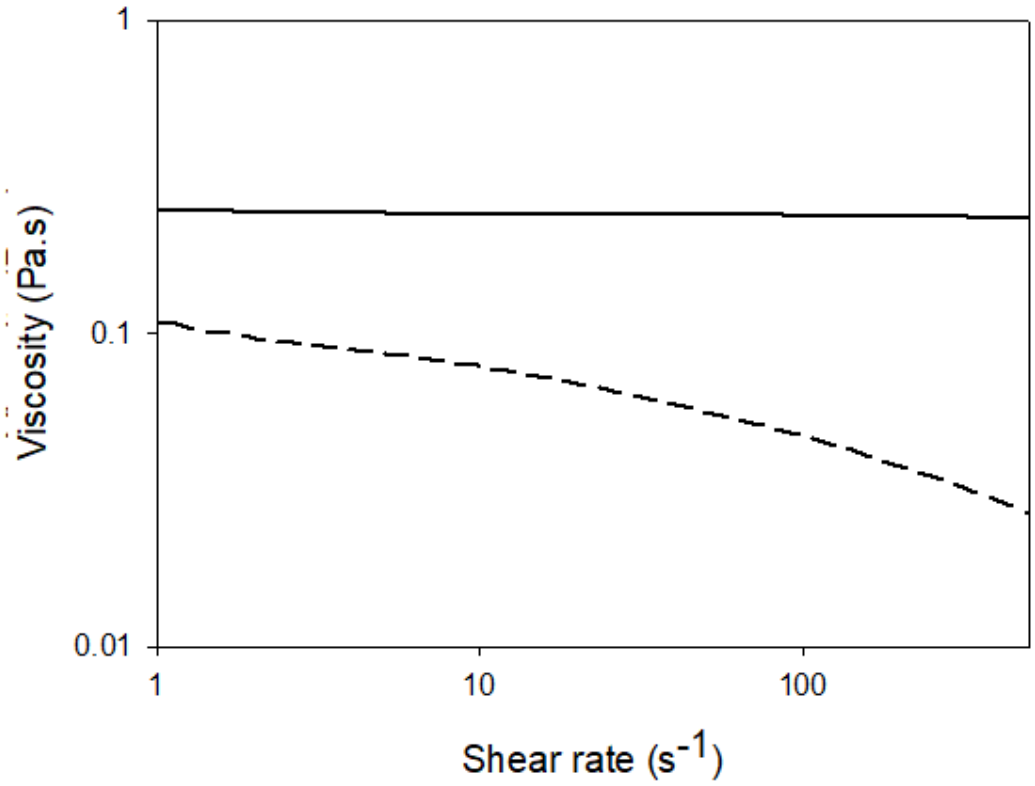

Fig. 4.

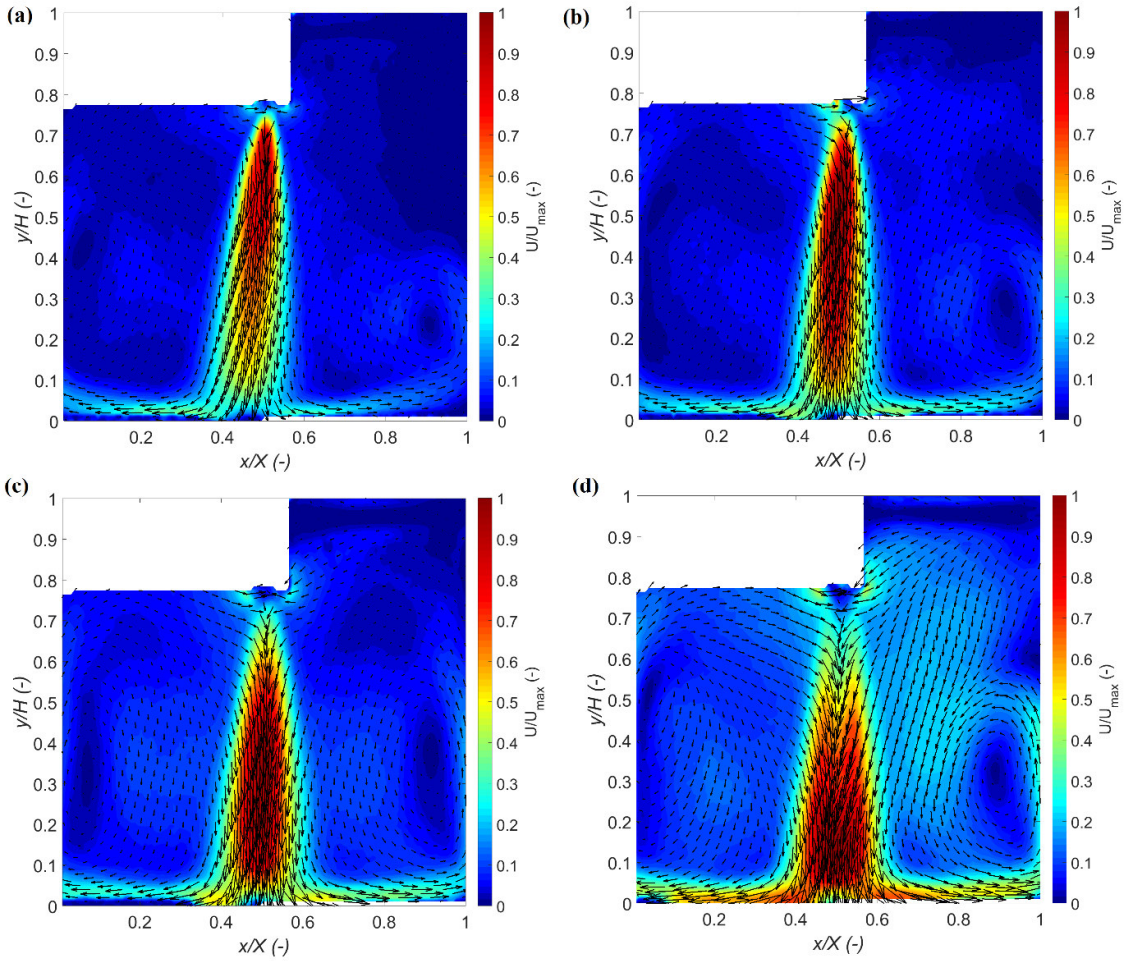

Fig. 5.

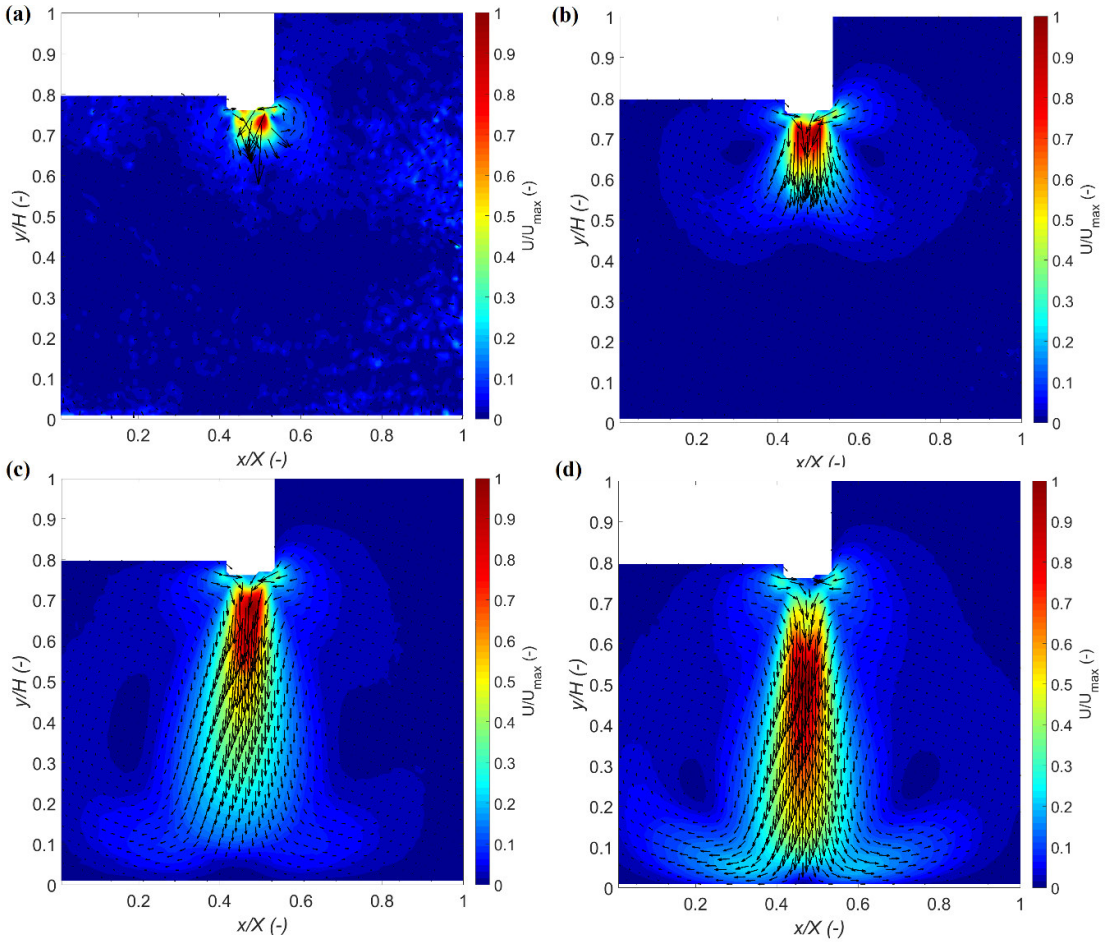

Fig. 6.

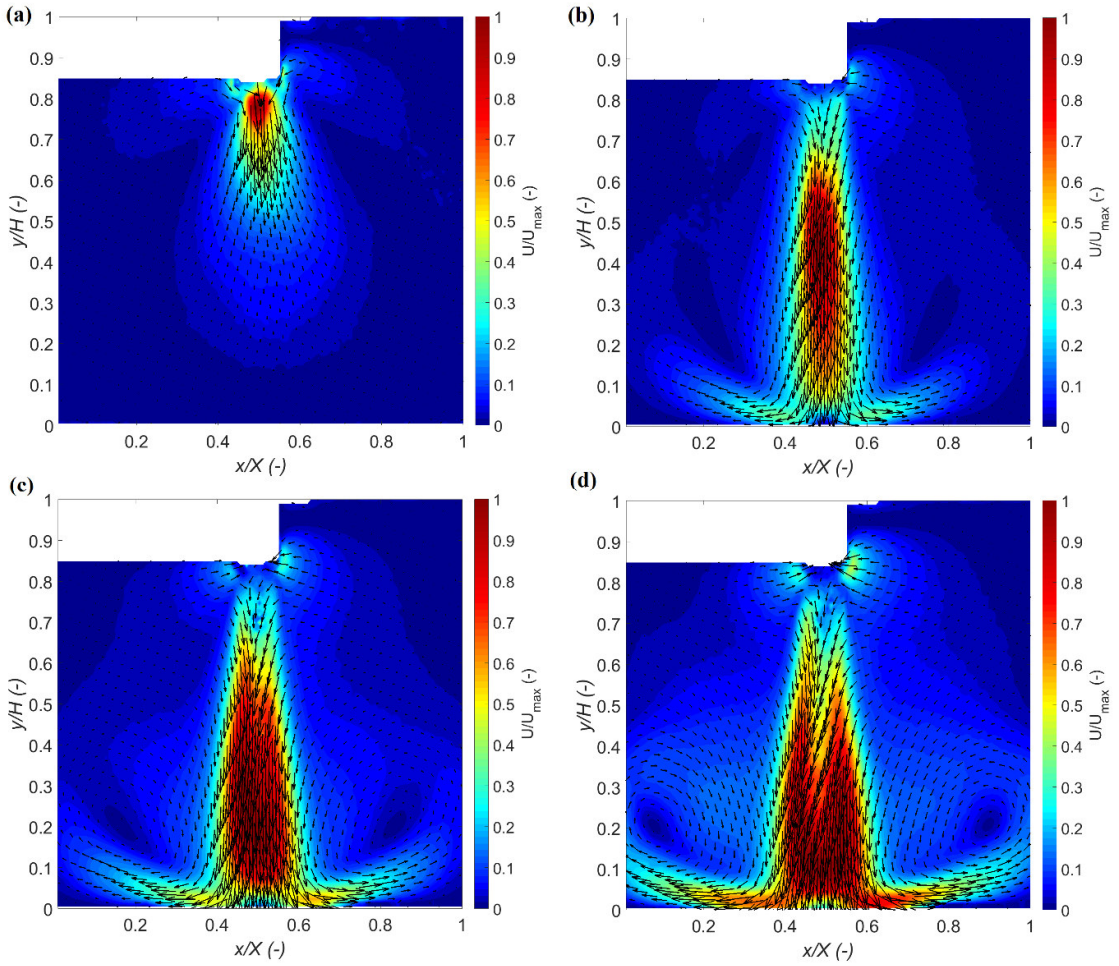

Fig. 7.

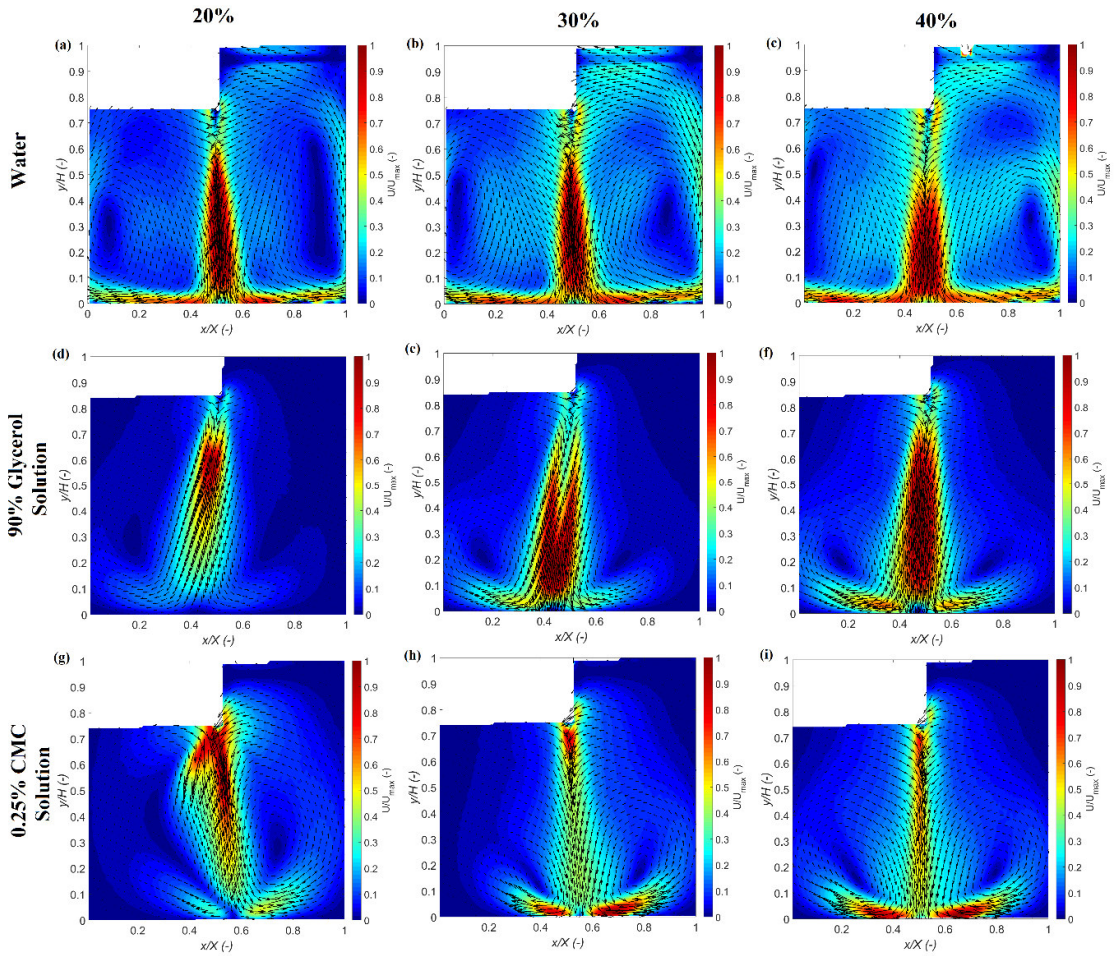

Fig. 8.

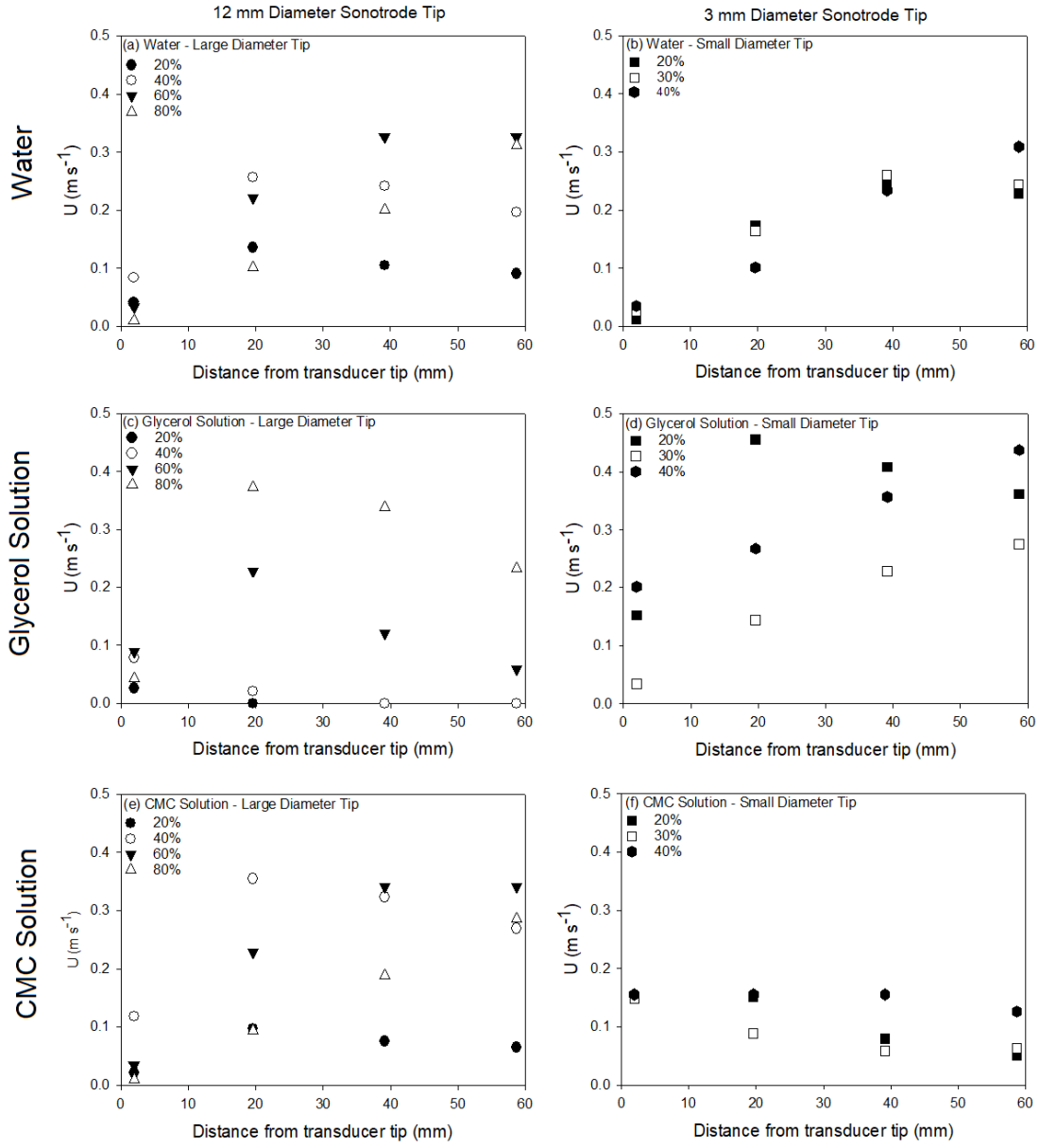

Tables

Table 1.

Ultrasonic amplitude, acoustic power and acoustic intensity for the microtip and larger tip configurations.

Ultrasonic tip diameter (d) and surface area (S_A)	Amplitude (%)	Acoustic power (W)	Acoustic intensity (W cm^{-2})
d = 3 mm S_A = 0.07 cm^2	20	8.5 ± 0.2	120.3 ± 2.8
	30	19 ± 0.6	269.1 ± 8.5
	40	32 ± 0.9	453.3 ± 12.8
d = 12 mm S_A = 1.13 cm^2	20	10.5 ± 0.7	9.3 ± 0.6
	40	23.1 ± 1.1	20.4 ± 0.9
	60	39.9 ± 1.6	35.3 ± 1.4
	80	49.7 ± 1.3	43.9 ± 1.2

Table 2.

Maximum velocity (U_{max}) as a function of transducer tip size, ultrasonic amplitude, and investigated fluid rheology.

		U_{max} (m s^{-1})		
Ultrasonic transducer	Ultrasonic amplitude (%)	Water	Glycerol Solution	CMC Solution
d = 3 mm	20	0.249	0.584	0.169
	30	0.266	0.574	0.196
	40	0.442	0.446	0.247
d = 12 mm	20	0.151	0.027	0.108
	40	0.262	0.104	0.358
	60	0.339	0.293	0.351
	80	0.329	0.423	0.304

Table 3.

Comparison of experimentally measured velocity by PIV ($U_{experimetal}$) and theoretically determined velocity from *Eq.* 4 ($U_{theoretical}$), as a function of ultrasonic transducer size, ultrasonic amplitude and investigated fluid.

		Water		Glycerol Solution		CMC Solution	
Tip diameter and depth	Ultrasonic amplitude (%)	$U_{experimetal}$ (m s^{-1})	$U_{theoretical}$ (m s^{-1})	$U_{experimetal}$ (m s^{-1})	$U_{theoretical}$ (m s^{-1})	$U_{experimetal}$ (m s^{-1})	$U_{theoretical}$ (m s^{-1})
d = 3 mm h = 1.95 mm	20	0.012	0.032	0.152	0.025	0.152	0.032
	30	0.027	0.047	0.034	0.037	0.149	0.047
	40	0.035	0.061	0.201	0.049	0.155	0.061
d = 3 mm h = 39.13 mm	20	0.243	0.031	0.409	0.024	0.079	0.031
	30	0.261	0.046	0.229	0.036	0.059	0.046
	40	0.234	0.059	0.357	0.047	0.155	0.059
d = 12 mm h = 1.95 mm	20	0.042	0.002	0.026	0.001	0.021	0.002
	40	0.084	0.003	0.078	0.002	0.118	0.003
	60	0.034	0.004	0.088	0.003	0.035	0.004
	80	0.009	0.005	0.042	0.003	0.009	0.005
d = 12 mm h = 39.13 mm	20	0.105	<0.001	0	<0.001	0.076	<0.001
	40	0.241	<0.001	0	<0.001	0.323	<0.001
	60	0.326	<0.001	0.121	<0.001	0.341	<0.001
	80	0.201	<0.001	0.339	<0.001	0.189	<0.001

Table 4.

Shear rate ($\dot{\gamma}$) and Reynolds number (*Re*) determined from *Eq.* 5, as a function of ultrasonic transducer size, ultrasonic amplitude and investigated fluid.

		Water		Glycerol Solution		CMC Solution	
Tip diameter and depth	Ultrasonic amplitude (%)	$\dot{\gamma}$ (s^{-1})	*Re* (-)	$\dot{\gamma}$ (s^{-1})	*Re* (-)	$\dot{\gamma}$ (s^{-1})	*Re* (-)
d = 3 mm *h* = 1.95 mm	20	1.76	37.28	11.78	2.29	7.13	5.73
	30	2.41	79.72	7.01	0.52	9.27	5.94
	40	2.46	106.01	3.45	3.03	8.42	6.07
d = 3 mm *h* = 39.13 mm	20	13.91	1461.38	11.69	12.36	5.81	5.72
	30	12.28	1562.53	24.25	6.94	3.06	3.69
	40	8.41	1404.65	18.02	10.79	9.32	12.43
d = 12 mm *h* = 1.95 mm	20	0.81	506.61	0.32	1.57	6.72	3.22
	40	1.76	10007.43	0.63	4.75	5.66	16.98
	60	4.41	407.38	1.69	5.32	16.71	6.37
	80	5.58	118.35	2.53	2.56	14.14	1.59
d = 12 mm *h* = 39.13 mm	20	7.21	3166.35	0	0	0.61	16.81
	40	14.61	7240.95	0	0	23.05	157.16
	60	16.42	9777.19	5.13	18.19	21.16	162.66
	80	14.27	6016.45	18.54	51.21	17.55	86.54

Highlights

- Acoustic streaming was visualised using particle image velocimetry (PIV).
- Two transducers were investigated with different diameters (3 and 12 mm).
- Three fluids were investigated: water, a glycerol solution and a CMC solution.
- Flow behaviour and velocity magnitudes were assessed for all studied conditions.
- Shear rates and Reynolds number were determined for each of the systems.